THE ASTROPHYSICAL JOURNAL, 224: 857-872, 1978 September 15 © 1978. The American Astronomical Society. All rights reserved. Printed in U.S.A.

A STUDY OF THE TAURUS DARK CLOUD COMPLEX

J. H. ELIAS

Hale Observatories, California Institute of Technology, Carnegie Institution of Washington
Received 1978 February 27; accepted 1978 March 10

ABSTRACT

A near-infrared survey has been conducted of nearly 20 square degrees of the Taurus dark cloud complex. Additional observations have been made of selected objects detected in this survey. These observations show that recently formed stars are spread throughout the cloud, and that these stars are primarily T Tauri stars or T Tauri-like stars. Two luminous objects are identified embedded in the reflection nebulae IC 359 and IC 2087. A new Herbig-Haro object is also described. The reddening law of the dark cloud material is discussed; it does not appear to be unusual in the infrared. Comparison of the young stellar population in Taurus with that in Ophiuchus suggests that the star formation mechanisms in the two regions are qualitatively different.

Subject headings: infrared: sources — nebulae: individual — stars: pre-main-sequence

I. INTRODUCTION AND OVERVIEW

The Taurus dark cloud may be the nearest major aggregate of dust and gas in which star formation is currently in progress. Numerous T Tauri stars provide visual evidence for this, as does the presence of several Herbig-Haro objects. The dark cloud complex extends over many degrees, and does not have a well defined center.

Infrared studies have been confined to surveys of small selected areas (e.g., Allen 1972; Allen and Penston 1975; Strom, Strom, and Vrba 1976) or to studies of optically selected objects, such as T Tauri stars (e.g., Rydgren, Strom, and Strom 1976). It was clear that a more extensive infrared survey would be useful since it offers the best chance of finding obscured high-luminosity objects, which appear to be rare in the Taurus clouds (see Strom, Strom, and Grasdalen 1975). Also, lightly obscured or visually bright objects are not seen preferentially in such a survey, so that a better idea of the total population of objects of various types within the dark cloud complex is possible.

Nearly 20 square degrees in the center of the complex were surveyed at both 1.6 and 2.2 μ m. Over 200 objects were detected which were brighter at 2.2 μ m than K = +7.5. Spectrophotometry at 2 μ m and broadband 1–20 μ m photometry were done on 30 of the objects in order to determine the spatial distribution and the nature of the young objects associated with the dark cloud complex.

The observations are described in § II, and the results of the survey and of the subsequent photometry and spectrophotometry are described in § III. These results permit unambiguous identification of the young stars associated with the cloud (§ IV), based mainly on the results of the infrared spectrophotometry, using procedures described previously (Elias 1978a, hereafter Paper I). The identified field stars can be used to derive the Taurus reddening law (§ V).

The observations of several of the more interesting objects are discussed in detail. A newly discovered infrared source associated with the reflection nebula IC 359 is discussed in § VI, and the infrared source associated with the reflection nebula IC 2087 (Allen 1972) is discussed in § VII. A third infrared source associated with the emission-line object Haro 6-10 (Haro, Iriarte, and Chavira 1953) is discussed in § VIII.

The observations of T Tauri stars associated with the Taurus dark clouds are discussed in § IX; these indicate that the near-infrared flux distributions of these stars can best be modeled by a hot dust envelope combined with a late-type stellar photosphere. The results of this paper are compared with the results of a similar study of the Ophiuchus dark cloud complex (Elias 1978b, hereafter Paper II) in § X. This comparison is combined with the results of other comparative studies of these regions (e.g., Rydgren, Strom, and Strom 1976; Vrba, Strom, and Strom 1976) to discuss the differences between the two regions.

II. OBSERVATIONS

The infrared survey was done using the 60 cm telescope on Mount Wilson during the 1974 and 1975 fall observing seasons. The total area covered was 19.7 square degrees (Fig. 1). The 1974 observations were done using the two-channel InSb system described in Paper I. In this system, bands corresponding approximately to the standard $1.6 \,\mu\mathrm{m}$ (H) and $2.2 \,\mu\mathrm{m}$ (K) filters were observed simultaneously with a 1' beam. Scans were done at sidereal rate, spaced 45" apart in declination. The chopping direction was parallel to the scan direction, and the beam spacing was roughly 2'. The limiting magnitudes were near $H = +7.5 \,\mathrm{and}\,K = +8.0$. These observations covered the region to the south of the dotted line in Figure 1b.

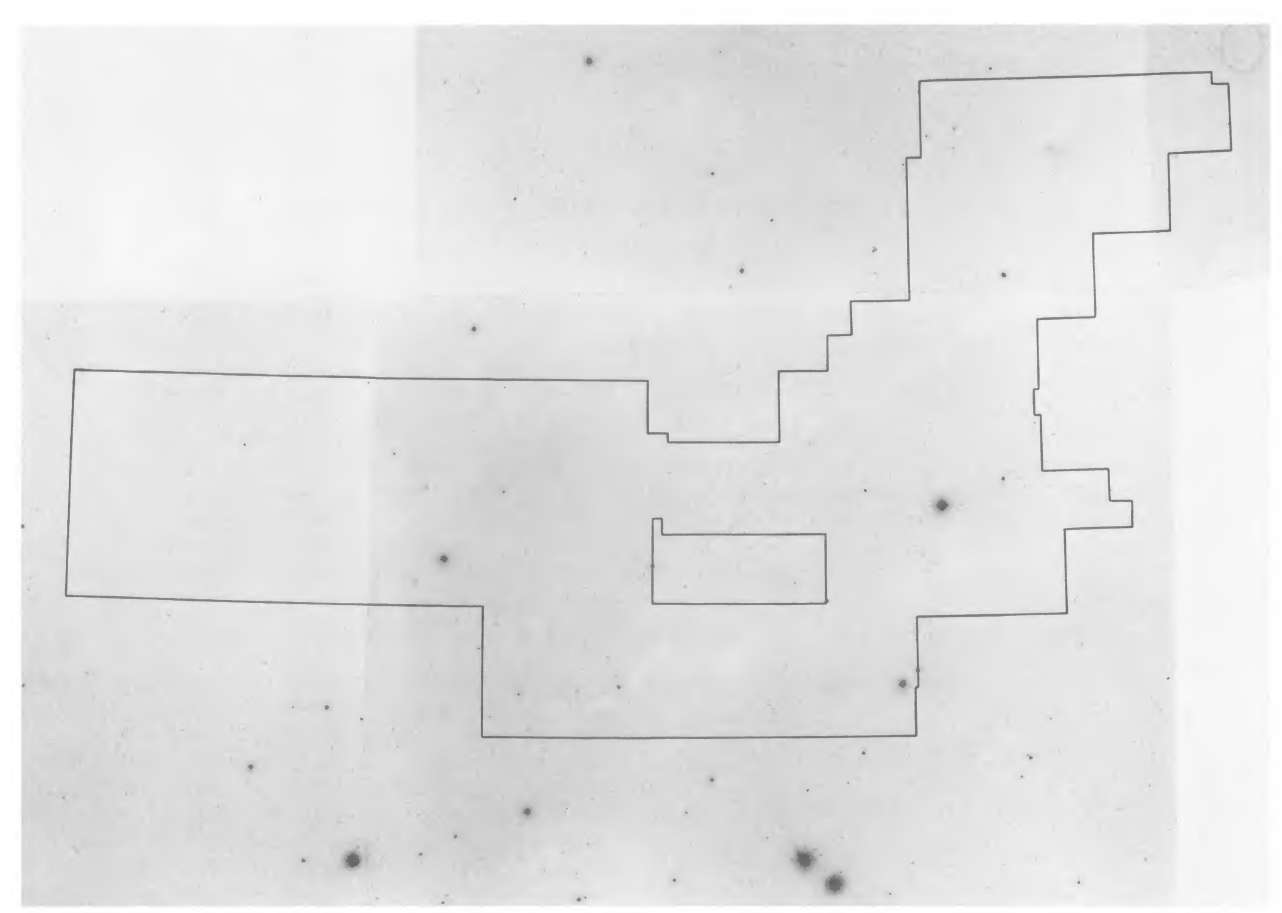
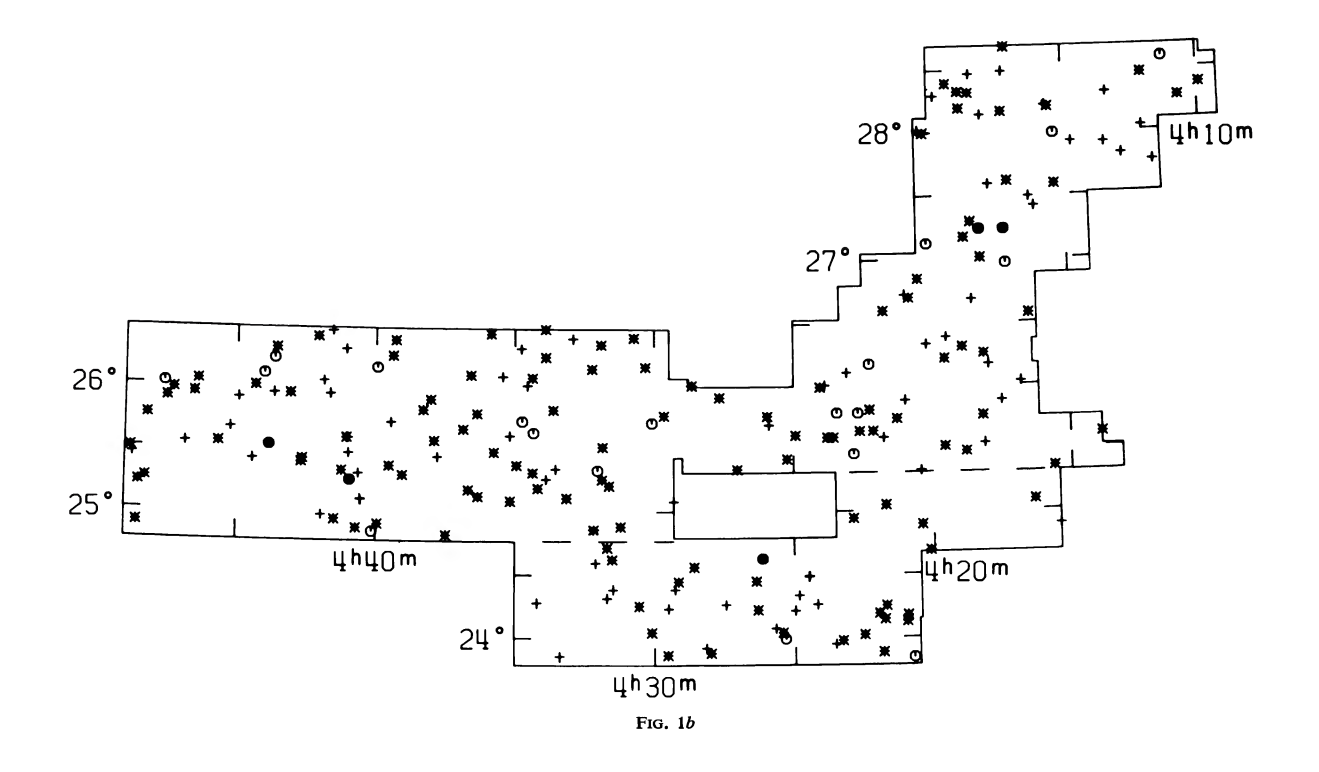


Fig. 1a



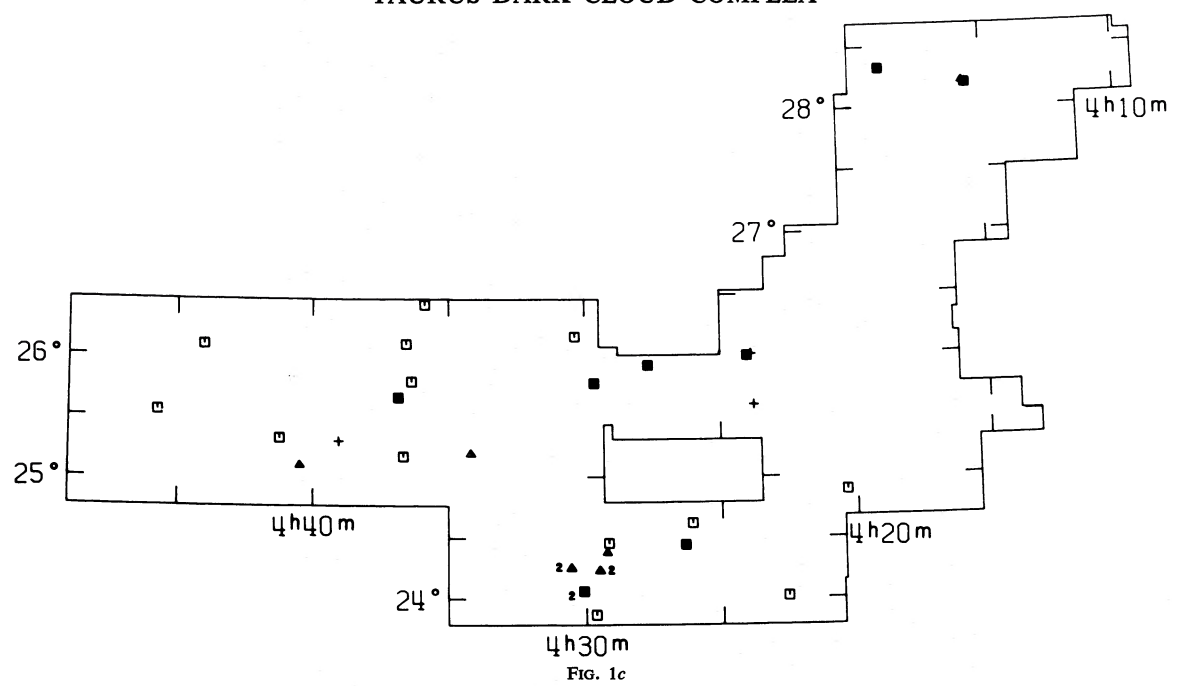


Fig. 1a.—Outline of area surveyed, superposed on a mosaic of Palomar Sky Survey blue prints. The maximum extent of the region is roughly 5° in declination and 9° in right ascension. The box in the center is a region omitted from the survey.

Fig. 1b.—Sources brighter than K = 7.5 detected in the survey. Objects with 7.0 < K < 7.5 are shown as pluses, objects with 5.0 < K < 7.5 are shown as asterisks, objects with 3.0 < K < 5.0 are shown as open circles, and the objects with K < 3.0 are shown as filled circles.

Fig. 1c.—Sources in Taurus which were studied in detail. Squares are objects with K < 7.0, and $H - K \ge 0.70$; triangles are the remaining objects in Table 1. The filled symbols are association members, and open symbols are field stars. The three pluses are T Tauri stars detected by the survey with K < 7.5 which were not subsequently observed. A "2" next to a symbol indicates that two objects from Table 1 are at that position.

The 1975 observations were done using the more sensitive system described in Paper II. This system was a single-channel InSb detector, with a 2' beam. Scans were done at both 1.6 and 2.2 μ m. Scanning was again done at sidereal rate, but with a spacing in declination between successive scans at the same wavelength of 1'.5. The beam spacing was approximately 3', and the limiting magnitudes were roughly H = +8.5 and K = +8.0.

Selected objects detected in the survey were observed using broad-band photometry from 1.2 to $20~\mu m$ and using low-resolution $2~\mu m$ spectrophotometry. These observations were made using the 0.6, 1.5, and 2.5 m telescopes on Mount Wilson. Most of the observations between 1.2 and 4.8 μm were made with an InSb detector; the remaining observations and the observations at longer wavelengths were made with a germanium bolometer. The properties of the various filters and the flux calibration used are given in Wilson et al. (1972), Beckwith et al. (1976), and Paper II. The calibration and reduction of the $2~\mu m$ spectrophotometry are described in Paper I.

Several deep infrared plates (IV-N emulsion + Wr88a filter) were taken on the 48 inch (1.2 m) Palomar Schmidt, primarily for purposes of identification of objects. This plate material was supplemented by several deep red (127-04 emulsion + red Plexiglas filter) plates which were made available by Dr. J. E.

Gunn. Dr. Gunn also provided optical spectra for two of the objects (see §§ VI, VII); these were taken using the Cassegrain SIT spectrograph on the 5 m Hale telescope.

III. RESULTS

a) Survey

The spatial distribution of the 215 objects found in the survey with K < 7.5 is shown in Figure 1b. Of these, 144 were brighter than K = 7.0. Detections in adjacent scans were considered to be due to a single source if they were coincident in right ascension by 2' or less. The actual counts must be corrected for pairs of stars occurring so close as to be considered one object, but this coincidence correction is less than 3% for all sources brighter than K = 7.5. The cumulative counts, corrected for coincidence, are shown in Figure 2.

b) Photometry and Spectrophotometry

Two groups of objects were observed more extensively. The first group consists of the 21 objects which were observed to have $H - K \ge 0.70$ and K < 7.0; as shown in Paper II, this appears to be a reasonable selection criterion for finding objects which are likely to be associated with the dark cloud material. These objects are listed in Table 1, together with previous

I ADLE I

MEASUREMENTS OF SELECTED OBJECTS

							INFR	INFRARED MAGNITUDES	UDES			10 рм	, m:	
OBJECT	IDENTIFICATION	α (1950)	6(1950)	POSITION	[1.2]	[1.6]	[2.2]	[3.4]	[4.8]	[10]	[20]	FILTER	SPECTRA	ASSOCIATION
2		9,7°m,21,47	+28°12'01"	0	8,55	6.91	5.64	47.4	3.84	0.54	-1.9±0.2	1,2	2	¥
: ;	DV Test	4 18 50.8	+28 19 35	HRC	8,12	6.82	5.68	4.37	3.6±0.1	1,0±0,1	-0.8±0.3	2	1	Ą
, c	ne tu	4 20 22.6	+24 53 13	0	8.25	6.57	5.82	5.38	>5.0	5.2±0.3			1	ĒΨ
7 4		4 22 37.4	+24 01 03	0	7.57	6.90	6.73	6.6±0.1		>5.7			1	ſz4
*	DG Tan	4 24 00.9	+25 59 36	HRC	9,22	7.88	6.75	5.08	4.1±0.2	1.7±0.1	-0.4±0.3	2	1	¥
*	IRC+20082	4 26 05.7	+24 37 17	0	5,35	3.70	2,86	2,23	2,30	1.42	+0.6±0.2	1,2	5	Œ.
*	Haro 6-10	4 26 22.0	+24 26 29	0	10.49	8.58	96.98	5.15	3.8±0.1	1.5±0.1	-0.9±0.2	2	. 2	Ψ.
. *	DK Tail	4 27 40,4	+25 54 59	HRC	9.31	8.16	7.17	5.81	5.1 ± 0.1	3.07	+1.4±0.4		- - ,	¥ I
0		4 29 09.6	+24 27 17	0	7.56	6.13	5.56	5.12	5.1±0.2	4.8 ±0.2			⊶.	Eu I
10		4 29 37.7	+23 52 07	0	7.71	6.54	00.9	5.44	5.5±0.2	×5.1			-	.
,	1	000	77	Odn	1.7 O	7 60	7 02	6 4+0 1	5 6+0 3	7.0+0.7			1	¥
11*	UZ Tau t&p	4 29 39.2	9 6	DE C		20.7	70.7	6 27	7 0+6 9	2 3+0 2			-	Ą
12*		4 30 05.2	S	0	0.10	00.7	9.0	17.0	† O-0-0	1.0-0-0				Ĺ×
13		8	60	0	8,48	6,55	5.58							. 6
14		4 35 53,4	22	0	9.29	7.67	96.9						٠,	. , [:
15	Allen & Penston (1975)	4 36	41	0	10.74	8.21	68.9	6.2 ± 0.1					٠,٠	ı, [
16		4 36	05	IR	10.14	6.90	2.06	4.09	3.9 ± 0.1	3.7±0.1			7 .	. .
17		4 36 40.6	10	0	8.53	7.22	6.61	6.2 ± 0.1		7.7		ď	(.
18*	IC 2087 (Allen 1972)	4 36 51.8	+25 39 13	0	10.8±0.2	8.21	6.25	4.49	3.4±0.2	2.4±0.2		7	უ -	e u
19		41	19	SO	7,54	74,	20.9	5.8±0.1	5.7±0.3	5.4±0.3		·	٦ ,	i [
50×	RV Tau	4 44 01.9	02	AGK3	77.9	5.71	4.97	3,45	2,45	0.3±0.1	-0.6±0.3	7	7	4
21		4 45 44.1	+25 32 59	SO	7.82	6.67	6.27	5.94	6.1±0.4	>5.5			1	ít.
33	Hibble 4		12	0	8.52	7.61	7.26	7.4±0.4	>5.0	6.4			1	A
23*	Haro 6-13		52	0	10.22	8.67	7.46	6.0±0.1		4,3±0,3			_	Ą
. 7	FY Tan	5	13	0	10,12	8.99	8.23	7.5±0.2					0	¥
2 Y	F2 Tau		13	0	9.93	8.64	7.64	6.2 ± 0.1		4.6±0.3	9.07		0	¥.
3 %	GH Tan	30	03	HRC	9.24	8.30	7.72	7.0±0.1		5.6±0.3	9.04		0	Ą
27	GI Tau	8	15	HRC	9.27	8,33	7.68	>6.3		3.8 ± 0.1	¥]:1		0 (Α.
78	GK Tau	8	14	HRC	9.29	8.17	7.35	6.4±0.3		4.0±0.2			o •	Κı
56		4 34 12.0	+25 11 30	0	8.14	7.20	98.9	6.5±0.2					F	24 D
8			90	SO	8.74	7.66	7.32	6.9±0.2					-	4

TABLE 1 (CONTINUED)

Description of Table l

An asterisk following the number indicates a note for the object follows the table, Object number used for identification in the text. Object. Column 1

stars generally follow Herbig and Rao (1972) and Herbig (1977) identifications of T Tauri Notation and Previous identification of the object. Column

in (5)

The origin of the positions is given 150), 6(1950), Position. Coordinates for equinox 1950. The origin o Optical position measured from 48-inch Schmidt plates taken in 1976. Columns 3-5

Optical position measured from a glass duplicate of the Palomar Sky Survey plate El461. Position taken from Herbig and Rao (1972). $\alpha(1950)$, 6(1950), 0: Optical positi OS: Optical positi HRC: Position tak

No counterpart visible on plates, position determined from photometer offset guider settings. Position taken from the AGK3. No correction for proper motion applied.

Uncertainties are given explicitly for magnitudes given to mag. Infrared Magnitudes. Magnitudes given to two decimal places are uncertain by less than ± 0.10 decimal place. Upper limits are 3 σ upper limits. 6-12

10pm Filter Set. Filter set or sets used for narrowband 10 µm photometry. Measured magnitudes are given in the 13 Column

Number of 2 µm spectra obtained, Column 14 2 µm Spectra.

cloud, Associated with the dark text for definitions Field star. F: : Column 15 Association.

Remarks (by object number)

- ble illuminating object for IC359 (see $\sqrt[9]{VI}$). Magnitudes listed are averages for the period 1976 February-December, during which no significant variations were seen. tar was significantly fainter 1977 December 6 (UT), with [1.2] = 8.70, [1.6] = 7.17 and [2.2] = 6.07. Mean values for 1976 for 10 µm narrowband filters, set #2 are = 1.49, [9.3] = 1.01, [10.9] = 0.14, and [12.2] = -0.11. Measurements with 10 µm filter set #1 are similar but less accurate. Possible illuminating object for IC359
- $[8.5] = 1.7 \pm 0.1$, $[9.3] = 1.2 \pm 0.1$, $[10.9] = 0.8 \pm 0.1$, and $[12.3] = 0.7 \pm 0.1$. um narrowband magnitudes, set #2, are: 2 5
- Probably variable. Measurements listed are for 1976 December 20 (UT), and include 10 µm narrowband measurements (set #2): [8.5] = 2.3 \pm 0.1, [9.3] = 2.1 \pm 0.1, [10.9] 1.6 \pm 0.1, and [12.2] = 1.1 \pm 0.1. Measurements on 1976 November 2 are: [1.2] = 9.02, [1.6] = 7.78, [2.2] = 6.57. Š.
- ; ; May be variable by roughly ± 0.07 mag from 1.2 to 4.8 µm. Values tabulated are means at all measurements. 10 µm narrowband measurements are (average of sets #1 [8.5 + 8.7] = 1.77, [9.3 + 9.5] = 1.60, [10.9 + 11.2] = 1.08, [12.2 + 12.5] = 0.73. •
- measurements (set #2) for this date are: $[8.5] = 2.1 \pm 0.1$, [9.3]nts 1976 November 1 and 4 (UT). 10 μm narrowband meas Other measurements are described in the text (§VIII). Measurements given are mean of measurements 1976 November 1 and 4 (UT). [10.9] = 1.4 \pm 0.2, [12.2] = 0.9 \pm 0.1. Other measurements are describe Variable. 2.0 ± 0.2 , .
- Ē at 2.2 mag Mean of measurements between 1976 October and 1976 December; may have been slightly variable (amplitude $<\pm~0.1$ œ.
- Measurements for 1976 November 1 and 6 (UT) y star (4" separation); measurements are for both components. Measurements are for 1976 December 18 (UT). = 8.72, [1.6] = 7.83, [2.2] = 7.26, [3.4] = 6.29, and $[10] = 3.7 \pm 0.2$. Ξ.
- This object lies ~ 20" N of GH Tau (object #26). Possibly slightly variable, but amplitude must be < ± 0.1 mag at 2.2 µm. 12.
- 10 µm narrowband measurements an extended component (probably reflection nebulosity) at $\lambda \le 2.2$ µm, so measurements given are only those with a 9" beam, are: [8.5] = 2.9 ± 0.2 , [9.3] = 2.7 ± 0.2 , [10.9] = 2.6 ± 0.2 , [12.2] = 1.9 ± 0.2 . See §VII. Contains 18.
- Variable. Measurements tabulated are for 1976 December 20 (UT). 10 µm narrowband measurements (set #2) for this date are: [8.5] = 0.7 ± 0.1, [9.3] = 0.5 ± 0..., [10.9] = 0.1 ± 0.1, [12.2] = 0.1 ± 0.1, [12.2] = 0.1 ± 0.1, [12.2] = 0.1 ± 0.1, [12.2] = 0.1 ± 0.1, [12.2] = 0.1 ± 0.1, [12.2] = 0.1 ± 0.1, [12.2] = 0.1 ± 0.1, [12.2] = 0.1 ± 0.1, [13.4] = 3.0 ± 0.1, [13.4] = 3.0 ± 0.1, [13.4] = 3.0 ± 0.1, [13.4] = 0.5 ± 0.1, [13.4] = 0.5 ± 0.1, [13.4] = 0.5 ± 0.1, [13.4] = 0.5 ± 0.2, [13.4] = 0.5 ± 0.2, [13.4] = 0.5 ± 0.1, [13.4] = 0.5 ± 0.2, [13.4 20.
- Variable. Measures tabulated are for 1975 October 29 (UT). Additional measurements on 1976 August 30 are [1,2] = 11.18, [1,6] = 9.35, [2,2] = 7.95. 23.

862 ELIAS Vol. 224

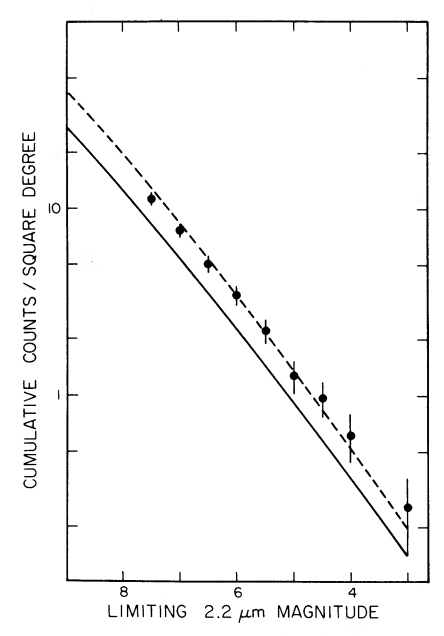


Fig. 2.—Cumulative 2.2 μ m source counts. The points show the observed counts, the solid curve shows the results predicted by the model in Paper I, and the dashed curve shows the results predicted if there is no radial decrease in stellar density toward the galactic anticenter.

identifications, positions, and infrared magnitudes. The distribution of these objects is shown in Figure 1c. The second group consists of nine objects which were observed for a variety of reasons; all are either fainter or bluer than the objects in Table 1. These objects are also listed in Table 1, as objects 22-30, and their positions are also plotted in Figure 1c.

Published values for the positions quoted in the table were used if available. Otherwise, the positions were measured from the Schmidt plates used for identification or were derived from the infrared photometer offset guider settings and measurements of guide star positions. The positions determined in this work are accurate to $\pm 1''$ if measured from plates, or to $\pm 5''$ if determined from offset guider settings.

The magnitudes listed in the tables are averages of all observations, unless the objects appeared variable. In these cases, only the most extensive single set of observations is listed and the additional results are given in the notes. Objects were not considered variable unless the differences in the $2.2 \,\mu\mathrm{m}$ measurements were greater than 0.15 mag. The photometry of those objects which have been previously studied by other investigators is in reasonable agreement with the earlier results (e.g., Mendoza 1968; Allen 1972; Gehrz 1972; Allen and Penston 1975; Rydgren, Strom, and Strom 1976).

The 2 μ m spectra of the objects in Table 1 are shown in Figure 3. The energy distributions of selected objects are plotted in Figure 4.

IV. ASSOCIATION MEMBERS

The criteria used to select objects from the survey for further study were intended to preferentially select young stars associated with the dark cloud. It is necessary to determine which of these objects are field stars before they are discussed in detail. It is also useful to estimate the number of stars associated with the cloud which were detected in the survey but were not observed further.

a) Identification of Young Stars

Most of the objects detected in the present survey appear to be field stars. This is best seen from the observed spatial distribution of the detections (Fig. 1b). The cumulative counts are in rough agreement with those predicted by the model of the galactic stellar distribution described in Paper I (Fig. 2), although it appears that the decrease in stellar density toward the galactic anticenter may be smaller than was supposed.

The predicted relative proportions of the various stellar spectral types are not sensitive to the scale length of the density decrease; consequently the predictions may be used with some confidence. According to these predictions, slightly under 90% of the field stars should be giants of spectral type G8 or later, and the remaining field stars should mainly be main-sequence A and F stars. The late-type giants should have a discernible CO absorption feature in their 2 μ m spectra longward of 2.3 μ m (Paper I) while the young stars associated with the cloud should have relatively featureless 2 μ m spectra. The main-sequence field stars will generally be unreddened foreground objects, and can therefore be identified by their "blue" colors. The identifications of the objects in Table 1 as field

The identifications of the objects in Table 1 as field stars or as objects associated with the dark clouds are given in the last column of this table. The identifications based on the infrared measurements were supplemented using lists of T Tauri stars and probable T Tauri stars (Haro, Iriarte, and Chavira 1953; Herbig and Rao 1972; Herbig 1977), and by searches for visible reflection nebulosity using the identification plates and searches for infrared reflection nebulosity using multiaperture infrared photometry. In addition to the stars in Table 1, three probable T Tauri stars were detected in the survey with K < 7.5, but were not observed further; these are DF Tau, FV Tau, and LkH α 332.

b) Properties of the Young Stars

The stars which are identified as association members are seen to be uniformly scattered over the entire region surveyed (Fig. 1c); there does not seem to be any single pronounced clustering of objects. There appear to be at least two small groupings of young stars. The first is to the northwest, including objects 1 and 22 and several T Tauri stars fainter than the infrared survey limit. A second clustering of young stars exists around $\alpha(1950) = 4^h30^m$, $\delta(1950) = +24^\circ$, and includes object 12 and objects 23–28. Several isolated young objects are also found, most notably

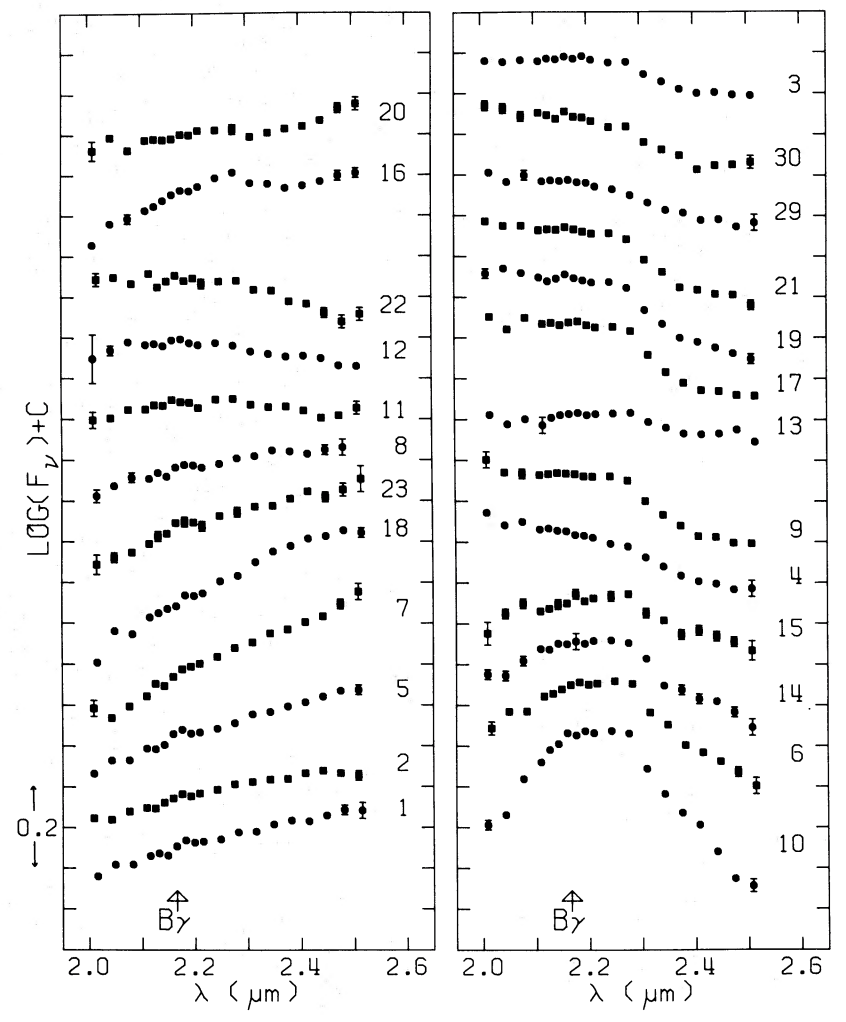


Fig. 3.—2 μ m spectra of objects in Table 1, identified by entry number in the table. The spectra have been shifted vertically by an arbitrary amount.

DG Tau (object 5), Haro 6-10 (object 7), and Allen's source in IC 2087 (Allen 1972: object 18). There are in addition well-studied groupings of young objects outside the survey region. The best examples of these are the groupings associated with XZ Tau and HL Tau, and with AB Aur and SU Aur (Strom, Strom, and Vrba 1976).

c) Field Stars

The field stars from Tables 1 and 2 are mostly normal late-type giants. The only exception to this is the variable star RV Tau (object 20), which has previously been studied in the infrared by Gehrz (1972). It is possible to see a weak CO absorption feature in the $2 \mu m$ spectrum of this object (Fig. 3), although it is much weaker than that seen in a normal late-type giant of similar spectral type. This provides additional support for the belief that most of the near-infrared flux from this star and other related objects does not come directly from the central star (e.g., Gehrz 1972).

V. REDDENING LAW

a) Derivation

The reddening law for Taurus was derived in a manner similar to that used in Paper II. A spectral type was assigned to each of the normal field stars listed in Table 1 based on the depth of the $2.3 \mu m$ CO band (see Paper I). Intrinsic colors for the stars were taken from Johnson (1966), as supplemented by Lee (1970) and Frogel *et al.* (1978); these colors were applied to the observed colors to obtain color excesses, which are listed in Table 3.

In order to obtain an idea of how the reddening law behaves at shorter wavelengths, approximate magnitudes were obtained from the Palomar Sky Survey prints for the stars in Table 2 which are located in the 4^h20^m, +24° field. These magnitudes were obtained using a magnitude-image-diameter relation calibrated using the photoelectric sequence of

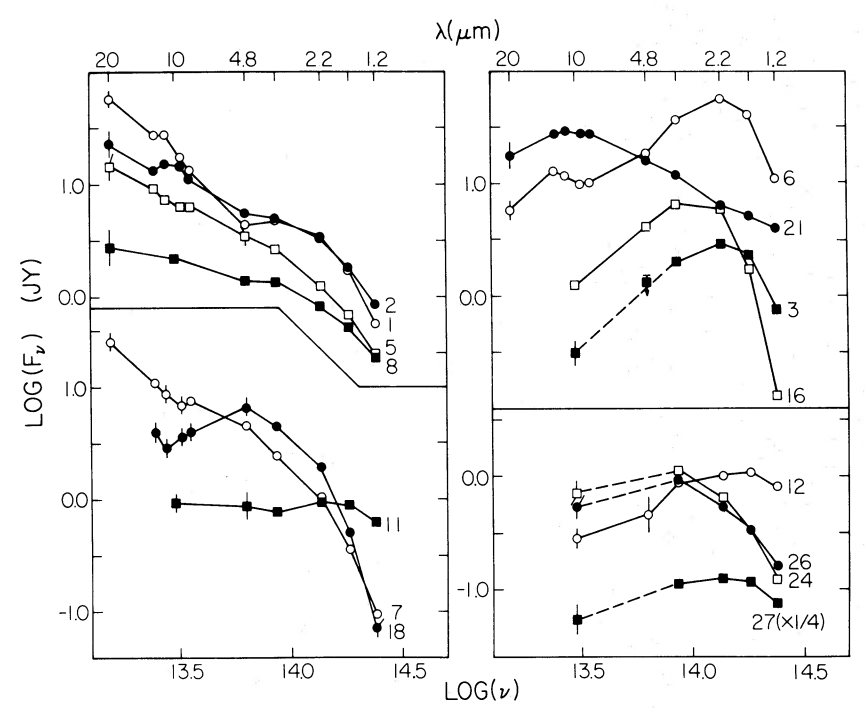


Fig. 4.—Energy distributions of selected objects from Table 1. Uncertainties are not shown if they are comparable in size to the symbols plotted. Curves are identified by the corresponding entry number in Table 1.

Landolt (1967) in this field. The photographic b magnitude was assumed equal to the photoelectric B magnitude for the sequence stars, while the photographic r magnitude was assumed to be given by the relation r = V - 0.49(B - V) given by Dorschner et al. (1966). The scatter about the relation indicated that the photographic magnitudes are accurate to about ± 0.4 mag. A more accurate determination of the magnitudes was not needed, as the uncertainties in the intrinsic b - K and r - K colors of the individual stars are 0.5 mag or greater. The magnitudes for the

seven background stars which have optical counterparts are given in Table 3, along with the color excesses inferred from the measurements and the adopted spectral types. Images which are near the plate limit have been indicated as limits 1 mag brighter than the approximate plate limit. Weighted means of the color excess ratios are listed in Table 4. For comparison, the mean values for the Ophiuchus dark cloud (Paper II) are given, together with values for the interstellar medium in the direction of the galactic center (Neugebauer et al. 1978; Becklin et al. 1978).

TABLE 2
FIELD-STAR INFRARED COLOR EXCESSES

	Color Excesses (mag)			Car can Ar			
Овјест	E_{J-H}	E_{H-K}	E_{K-L}	E_{K-M}	E_{K-N}	SPECTRAL TYPE	A_v * (mag)
3	1.12	0.65	0.30		0.7 ± 0.3	K2 III	8.1
4	0.16	0.09	0.01			K0 III	1.2
6	0.76	0.46				M8 III	5.9
9	0.62	0.34	0.24			M4 III	4.5
10	0.28	0.17				M8 III + †	2.1
13	1.37	0.87	• • • •			K2 III	10.3
14	0.72	0.45		90		M5 III	5.4
15	1.76	1.14	0.53	•••	• • •	M2 III	13.3
16	2.70	1.74	0.84	1.3 ± 0.2	1.5 ± 0.2	K1 III	20.6
17	0.45	0.35	0.18			M5 III	3.7
19	0.29	0.14	0.06	• • • •	- 1 ·	M4 III	2.2
21	0.38	0.22	0.16			M2 III	2.6
29	0.44	0.27	0.20±			G9 III†	3.2
30	0.57	0.26	0.29‡	• • • •		KO III†	3.8

^{*} $A_V = 4.6E_{J-K}$.

[†] Spectral type uncertain.

[‡] Value uncertain.

TABLE 3
FIELD-STAR COLOR EXCESSES

-		GRAPHIC NITUDE*	Color Excesses†		
Овјест	ь	r	E_{b-K}	E_{r-K}	
3 9 13 14 15 17	≥ 20‡ 17.7 > 20\$ > 20\$ > 20\$ ≥ 20‡ 15.5	13.5 13.8 14.2 15.9 ≥21.5∥ 15.2 12.6	≥10.4 5.2 >10.6 > 5.2 > 5.6 5.4	5.7 4.2 6.6 4.2 ≥11.4 3.9 4.0	

- * Uncertainty ±0.4 mag.
- † Uncertainty ± 0.7 mag.
- ‡ Marginally visible.
- § No image visible.
- || No image visible on red print, but a faint image is seen on a deep 127-04 plate.

The reddening law at 4.8 μ m and longwards is based essentially on measurements of one object, number 16, as there are no other objects with accurately measured magnitudes for which intrinsic colors are known. As the color excess ratios are roughly consistent with an extinction law proportional to λ^{-1} , it will be assumed that $A_K = 1.1 E_{H-K}$. This value is quite arbitrary, but it is unlikely that it is severely in error. The extinction at 2.2 μ m cannot be less than the K-N color excess, and the extinction at 10 μ m of object 16 cannot be greater than 1.5 mag, as its implied brightness would not be at all consistent with its spectral type and a position on the far side of the dark cloud. The limits on the 2 μ m extinction are therefore $0.9E_{H-K} < A_K < 1.8E_{H-K}$.

b) Results

There seem to be no significant differences in the infrared between the three reddening laws listed in Table 4. There is not enough information to find small differences between one reddening law and the next, but large deviations from a "normal" law can be excluded. This result is in contrast to those of Grasdalen (1974) and Rydgren, Strom, and Strom (1976), who find dark cloud reddening laws which are very different from that found here. The main difference is that previous determinations have used stars embedded in the dark clouds, rather than background stars, to determine the reddening law. The difference between the resulting reddening laws can be ascribed to unusual reddening in the immediate vicinity of the embedded stars due to modification of the grains by the stellar radiation or to formation of unusual grains in a stellar wind.

The observed unusual reddening laws can equally well be explained by a normal reddening law combined with a near-infrared excess (e.g., Garrison 1968). Most of the objects for which unusual reddening laws are derived show definite excesses at $10 \,\mu m$ and longer wavelengths. It will be assumed that the reddening law derived above applies to all objects discussed in this paper. In general, however, the conclusions in

TABLE 4
REDDENING LAWS

		REGION	
Color Excess Ratio	Taurus Dark Cloud	Galactic Center*	Ophiuchus Dark Cloud†
$E_{J-H} E_{H-K}$ $E_{K-L} E_{H-K}$ $E_{K-M} E_{H-K}$ $E_{K-M} E_{H-K}$ $E_{r-k} E_{H-K}^{+}$ $E_{B-K} E_{H-K}^{+}$ $A_{K} E_{H-K}$ $A_{V} E_{H-K}$	$\begin{array}{c} 1.56 \pm 0.05 \\ 0.48 \pm 0.03 \\ 0.75 \pm 0.10 \\ 0.87 \pm 0.10 \\ 9.7 \pm 0.8 \\ 16 \pm 3 \\ 1.1 \\ (+0.7, -0.2) \\ 128 \end{array}$	1.50 ± 0.09 0.65 ± 0.06 0.8–1.7	1.60 ± 0.04 0.56 ± 0.04 14

- * Neugebauer et al. 1978; Becklin et al. 1978.
- † Paper II and Vrba et al. 1975.
- ‡ r is the red Palomar Sky Survey magnitude.
- § Adopted value.

these discussions do not depend critically on the details of the reddening law which is assumed.

VI. OBJECT 1

The region around the three T Tauri stars CZ Tau, DD Tau, and Hubble 4 (object 22; see Herbig 1977) was identified as IC 359 by Hubble (1922). Struve (1937, 1961) and Struve and Swings (1948) noted that the three T Tauri stars were not apparently bright enough or blue enough to account for the extent and color of the surrounding reflection nebulosity. Grasdalen, Strom, and Strom (1973) suggest that the dominant illuminating star has to be another as yet undiscovered object, probably an early-type star. Object 1 is located in the middle of the nebulosity (Fig. 5 [Pl. 12]) and has an optical spectrum like a moderately reddened star with emission at $H\alpha$ (Fig. 6). It seems probable that this star is the source of the illumination for much of the reflection nebulosity surrounding it.

The star is not a normal main-sequence star, as it shows $H\alpha$ in emission (Fig. 6) and is variable in the near-infrared (Fig. 7). The brightness of the object in the red ($m_r \sim 15$) relative to that in the infrared suggests a visual extinction of roughly 10 mag. The maximum visual extinction consistent with the observed 1.2–1.6 μ m color is approximately 12.5 mag if the reddening law of Table 4 applies. The intrinsic energy distribution of the object is shown in Figure 8 for these two values of the visual extinction. There is obviously an infrared excess at wavelengths longer than 5 μ m, and it also appears that there is a significant flux excess over that expected from a hot star at wavelengths at least as short as 2.2 μ m.

There is no certainty that most of the flux below 2.2 μ m is entirely from the star. There is no evidence in the 2 μ m spectrum (Fig. 3) of the B γ line of hydrogen at 2.17 μ m, while the higher Balmer lines are seen strongly in absorption, with equivalent widths of ~ 20 Å (Fig. 6). The upper limit to the B γ absorption

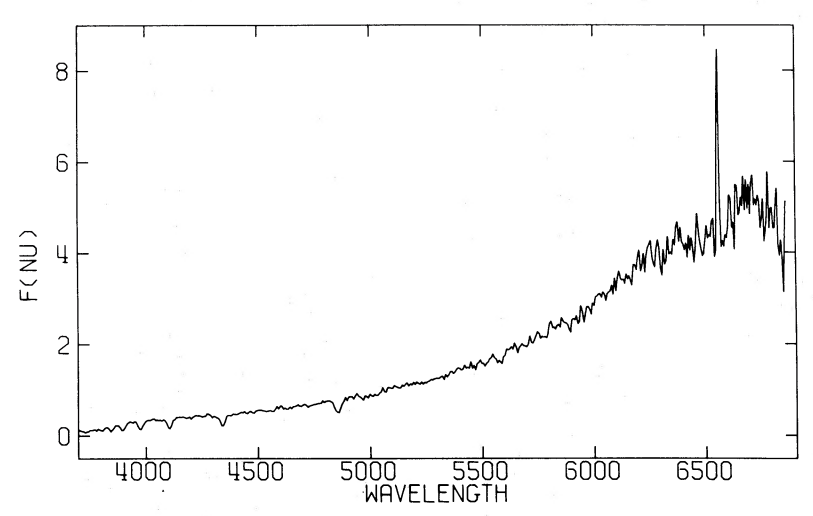


Fig. 6.—SIT spectrum of object 1. The flux scale is linear, but in arbitrary units as the spectrum was taken through a slit.

equivalent width is 5 Å, which suggests that most of the 2.2 μ m flux from object 1 does not come from the visible star, unless By emission is significant. On the other hand, the colors of the visual spectrum indicate that $B - V \sim 1.5$ mag and $V - r \sim 1.2$ mag; this implies a visual extinction of ~8 mag if the spectral type of the star is near A0. As this extinction is comparable to that inferred from the r - J color, it seems that the excess at 1.2 μ m is at most comparable to the stellar flux. If the 1.2 to 2.2 μ m excess is produced by dust with emissivity proportional to λ^{-1} and a grain temperature of 1500 K, the 1.2 μ m excess flux will be roughly a third of the 2.2 μ m excess. If this is the case, and if the visual extinction is 10 mag, roughly 85% of the flux at 1.2 μ m and slightly less than half of the flux at 2.2 μ m is from the star.

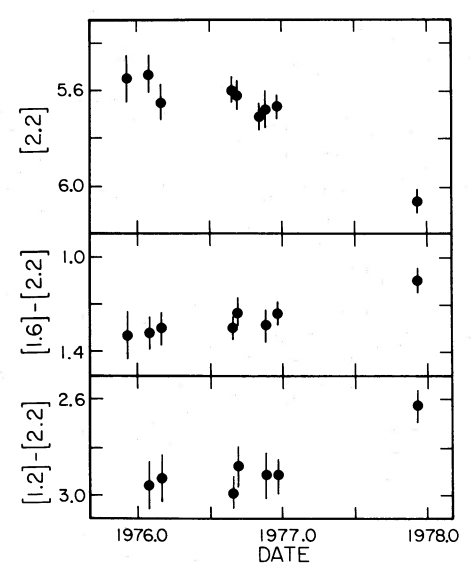


Fig. 7.—Infrared magnitudes and colors of object 1 as a function of time.

The simplest explanation of the observations is that object 1 is a Herbig Ae star (Herbig 1960) which is heating circumstellar dust. The heated circumstellar material is the probable source of the infrared flux; this material is either blown off from the star by a stellar wind or remnants of the material out of which the star condensed (Strom et al. 1972; Strom, Strom, and Grasdalen 1975; Paper I).

VII. IC 2087 (Object 18)

IC 2087 is a reflection nebula without a visible illuminating star (Struve 1937, 1961). The illuminating star (object 18) was discovered at $2.2 \,\mu m$ by Allen (1972), and additional photometry was done by Allen and Penston (1975) who also identified the optical counterpart on the Palomar Sky Survey red print. This star is more readily seen on deeper photographs (Fig. 9 [Pl. 13]) in the red and infrared.

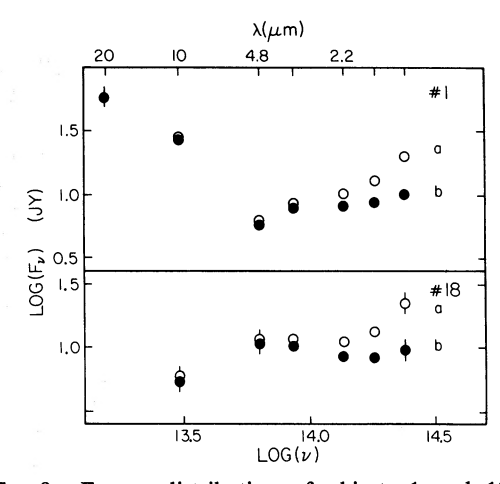


Fig. 8.—Energy distribution of objects 1 and 18 after correction for reddening using the law given in Table 4. The alternative values of visual extinction removed from object 1 are $A_V = (a)$ 12.5 mag and (b) 10 mag; the values removed from object 18 are (a) 20 mag and (b) 17 mag. Extinction at 20 μ m has been assumed to be negligible.

No. 3, 1978

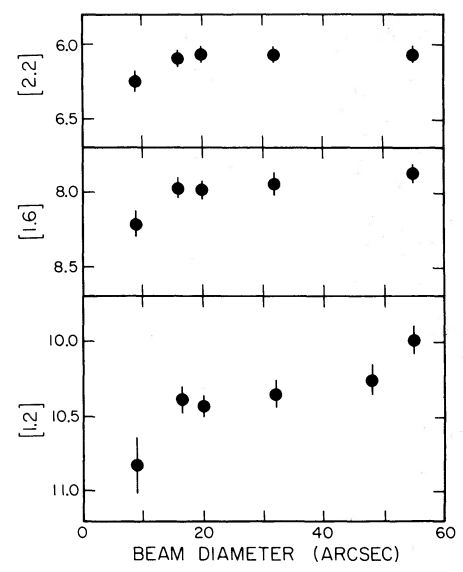
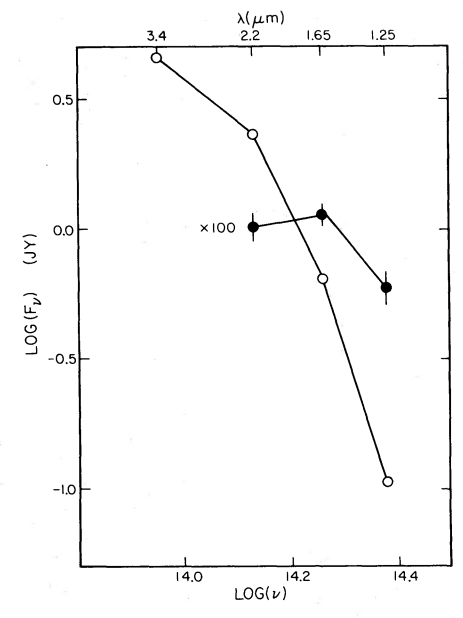


Fig. 10.—Multiaperture photometry of object 18. The measurements have not been corrected for flux in the reference positions. Chopper spacings and chopping directions are 14" east and west for the 9" beam, 30" north and south for the 20" beam, 48" north and south for 16", 32", and 48" beams, and 110" east and west for the 55" beam.

This object is the only object studied in Taurus which is significantly extended in the infrared (Fig. 10). This extended emission is presumably reflection nebulosity similar to that found around several objects in Ophiuchus (see Paper II). This suggestion is supported by the blueness of the extended emission, which is seen strongly at 1.2 μ m, and is only marginally detectable at $2.2 \mu m$. This blueness is shown more directly in Figure 11, where measurements of the nebulosity 32" east of the illuminating star are compared to measurements of the star. If the nebular spectrum is produced by a single scattering, the relative scattering crosssections Q_{λ} at 1.25, 1.65, and 2.2 μ m can be deduced from the colors. The value of $Q_{1.2}/Q_{2.2}$ is 13 ± 3 , and that of $Q_{1.6}/Q_{2.2}$ is 4.1 ± 0.8 . These values are consistent with the reflection being produced by Rayleigh scattering, for which the relevant values should be 9.6 and 3.2, respectively. As can be seen from Figure 9, the visual reflection nebulosity is brightest roughly 1' east of the infrared source. This suggests that the visual extinction decreases to the east of the object, which may be embedded near the eastern side of a dense condensation of dark cloud material. The blueness of the scattered radiation may then be due in part to reduced extinction along the line of sight to the east of the object.

The energy distribution of the object is not purely that of a reddened hot star. This can best be seen from Figure 8, where the energy distribution of the star is shown after correction for two alternative values of the extinction. The maximum visual extinction consistent with the measured 1.2–1.6 μ m color is ~20 mag; with this extinction removed, the object shows a significant flux excess at longer wavelengths. The



-Photometry of object 18 (open circles) and of a Fig. 11.—Photometry of object 18 (open circles) and of a position 32" to the east (filled circles, fluxes × 100), both with a 32" beam and 48" north-south chopper spacing. No corrections have been made for flux in the reference positions.

most probable extinction is ~ 17 mag. As with object 1, there may be a significant flux excess at all infrared wavelengths. The spectral type of object 18 is unknown; if the object emits little or no excess 1.2 μ m flux, and lies on the zero-age main sequence (ZAMS), it should have a spectral type of roughly B5. This is consistent with the radio continuum observations by Gilmore (1978), who found no detectable H II region surrounding the object; his limit indicates that the star has a spectral type later than B3. The star could well be considerably later than B5 if it lies above the main sequence, though the absence of detectable CO and H_2O absorption at 2 μ m (Fig. 3) implies a spectral type earlier than $\sim K0$.

VIII. HARO 6-10 (Object 7)

a) Description and Identification

The $H\alpha$ emission object Haro 6-10 (Haro, Iriarte, and Chavira 1953) is located in a region of the dark cloud relatively distant from any other identified young objects. Photographs of the object show it to be nonstellar (Fig. 12 [Pl. 14]), and a visual spectrum (Fig. 13) shows prominent [O I], [O III], and [S II] forbidden emission lines in addition to Balmer line emission. The appearance of the object and its visual spectrum strongly suggest that it is a Herbig-Haro (HH) object (cf. Herbig 1974; Haro 1976). This identification is supported by a more detailed comparison of the emission-line spectrum with that of other Herbig-Haro objects. The observed lines and their intensities are listed in Table 5, together with intensities corrected for plausible amounts of reddening. As a comparison, intensities observed by Böhm, Siegmund, and

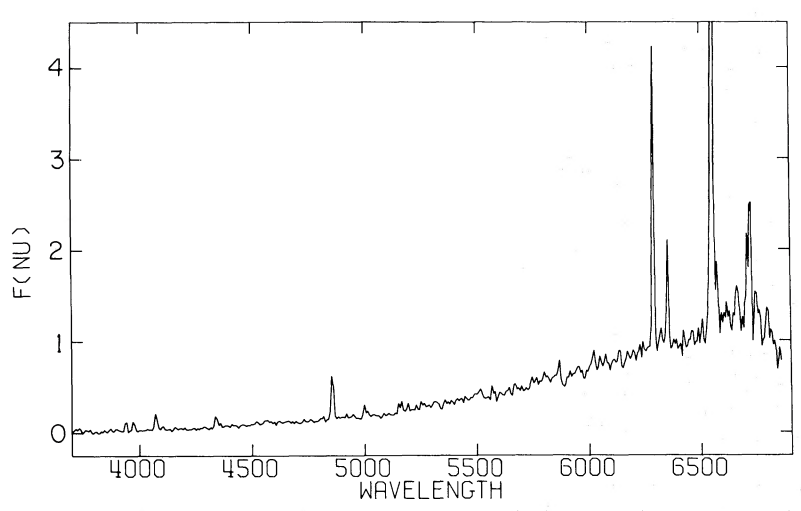


Fig. 13.—SIT spectrum of Haro 6-10. The flux scale is linear but in arbitrary units.

Schwartz (1976) for HH 1 are also listed, after correction for reddening.

The infrared source associated with Haro 6-10 is apparently very red (Fig. 4) and shows only a weak silicate feature. This suggests that it is intrinsically quite red. Infrared observations of this object cover a period of over 3 years, during which it has gradually grown fainter and redder (Fig. 14). A similar fading

has been observed on the plates of this object (Fig. 12). The maximum change in brightness at $2.2 \,\mu m$ has been roughly a factor of 3; the change in total observed luminosity has been considerably smaller, of the order of 30%, as most of the observed luminosity is emitted at the longer wavelengths, where the object is least variable. The infrared energy distribution of object 7 is very similar to those seen or inferred in

TABLE 5
OBSERVED LINE INTENSITIES IN HARO 6-10

*		Haro 6-10 (object 7)*	TTTT1+
Line	Observed	$E_{B-V}=1.0\dagger$	$E_{B-V}=1.5\dagger$	$- HH1\ddagger E_{B-V} = 0.6$
[O II] 3726+3729 H8 3889 Ca II 3933 Ca II 3968\\ Hε 3970\\ [S II] 4069+4076 Hδ 4101 Hγ 4340 [Mg I] 4562 [Fe III] 4814 Hβ 4861 [O III] 5007 He I 5016 [N II] 57555 He I 5876 [O I] 6300 [O I] 6300 [O I] 6364 Hα 6562 [N II] 6583 He I 6678 [S II] 6717 [S II] 6731	≤ 13 ≤ 8 30 ± 4 26 ± 4 48 ± 4 11 ± 4 29 ± 4 $13 \pm 6 \parallel$ $7 \pm 4 \parallel$ 100 6 ± 3 18 ± 3 $9 \pm 4 \parallel$ ≤ 12 $16 \pm 7 \parallel$ 323 ± 10 821 ± 25 65 ± 15 $40 \pm 20 \parallel$ 75 ± 20 135 ± 20	≤ 50 ≤ 24 84 ± 11 69 ± 11 111 ± 9 25 ± 9 49 ± 7 17 ± 8 7 ± 4 100 6 ± 3 16 ± 3 8 ± 4 ≤ 6 8 ± 3 120 ± 4 37 ± 4 266 ± 8 21 ± 5 12 ± 6 23 ± 6 40 ± 6	\leq 95 \leq 41 140 ± 19 113 ± 17 170 ± 14 37 ± 13 63 ± 9 20 ± 9 7 ± 4 100 5 ± 3 15 ± 2 7 ± 3 \leq 4 5 ± 2 22 ± 2 151 ± 5 12 ± 3 7 ± 3 12 ± 3	186 6 12 \$ 67 24 38 100 28 100 13 39 \$ 3 7 115 46 266 114 \$ 83 108

^{*} Normalized to $I_{\rm H\beta}=100$. The absolute intensities are not known.

[†] Observed intensities corrected for reddening using the Whitford reddening law (Miller and Mathews 1972).

[‡] Böhm et al. 1974, 1976.

[§] Not tabulated.

^{||} Uncertain detection and identification.

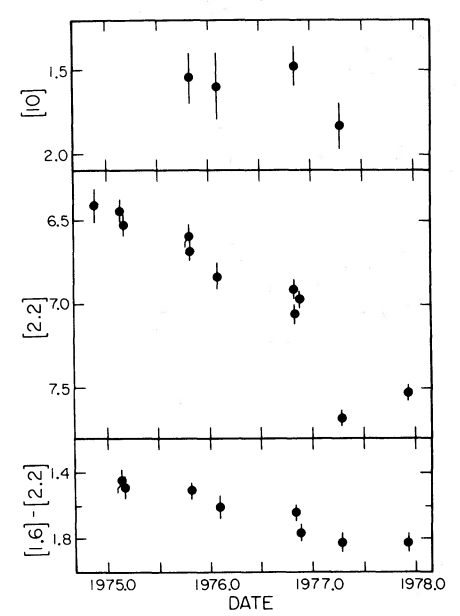


Fig. 14.—Infrared magnitudes and colors of Haro 6-10 as a function of time.

other Herbig-Haro objects (e.g., Strom, Grasdalen, and Strom 1974; Strom *et al.* 1976; Schmidt and Vrba 1975).

Haro 6-10 can be seen as a stellar object in the image tube guider used on the 1.5 m telescope, so it is possible to accurately determine the relative positions of the optical object and the infrared source associated with it. There is no evidence for any position difference greater than the centering uncertainty of less than 1".

b) Interpretation

The positional coincidence of the visible and infrared source positions strongly implies that the two are in fact the same object, and that the extinction derived from the visible spectrum applies to the infrared spectrum as well. The color of the optical continuum corresponds to a B - V color of ~ 1.8 , excluding the emission lines. The color excess, E_{B-V} , which is inferred from this depends on the mechanism producing the observed continuum. If the continuum is produced by optically thin recombination radiation, the color excess is ~ 1.4 mag for $T_e = 10^4$ K. If the continuum is optically thick, the excess is somewhat larger. The hydrogen lines in the spectrum can be used to derive an approximate reddening if it is assumed that they are produced by optically thin recombination; the resulting color excess is ~ 1.0 mag. This value may be considerably in error if the hydrogen emission lines are optically thick or if collisions are important. The estimates of E_{B-V} are thus all in the range 1–2 mag, and suggest that the total visual extinction is less than 10 mag. This relatively small value for the extinction indicates that the infrared energy distribution is intrinsically quite red. The visible continuum is therefore not produced by the same mechanism as the infrared flux. The energy distribution shortward of $2.2 \,\mu m$ may be affected by the "blue" component which produces the visible emission, and in this case the near-infrared variations may be produced by superposition of flux from a variable, blue component on a relatively constant, redder energy distribution. The structure of the object remains mysterious. One possibility is that the infrared flux is produced by heated dust outside or mixed with the emission-line region, in which case the source of excitation for the emission-line region is undetected. A more speculative alternative is that the infrared flux is from a stellar object inside the emission-line region which excites it in some way, possibly by means of mass loss and shock heating. Probably the best way to differentiate between the two possibilities is to measure the object's size in the infrared, in order to distinguish between a compact object and a more extended object with a size comparable to that of the core of the emission region, which is at most a few seconds of arc. The present measurements constrain the size at 10 µm to less than 7".

No other Herbig-Haro objects were detected in the survey. HH 31 (Herbig 1974) lies outside the region surveyed, but two candidate objects lie inside the boundaries. The most promising of these is Haro 6-19 (Haro, Iriarte, and Chavira 1953) which lies at $\alpha(1950) = 4^h29^m37^s6$, $\delta(1950) = 24^\circ15'08''$, and shows H α in emission. It is readily seen on red plates, where it is obviously nonstellar, but it is invisible on infrared plates. No infrared source was seen down to a limit of K = +8.0 at or near the position of this object. A second object is the small fuzzy patch visible in the red near IC 2087, about 3' to the northeast (Fig. 9); its coordinates are $\alpha(1950) = 4^h37^m04^s4$, $\delta(1950) = +25^\circ40'54''$. No spectroscopic information is available for this object, although it also has no detected counterpart on infrared plates or at 2.2 μ m.

IX. T TAURI STARS

The objects in Table 1 include over a dozen T Tauri stars and probable T Tauri stars. These objects show a considerable variety in their energy distributions (Fig. 4), indicating that they cannot be modeled simply. The observed distributions range from that of Hubble 4 (object 22), which has an energy distribution very nearly that of an ordinary late-type star, to that of DG Tau (object 5), which shows a much cooler energy distribution with only a negligible contribution by a stellar component. DG Tauri shows a weak $10~\mu m$ absorption feature, while RY Tau (object 2) shows a similar feature in emission. There is a tendency for some of the redder objects to show two distinct components in their energy distributions, which are then characterized by a dip at $3.4~\mu m$. Other objects show no such dip.

These objects are thought to be stars of moderately late spectral type (typically K or early M) surrounded by a circumstellar emission envelope. This envelope clearly contains a certain amount of ionized gas, indicated by the presence of emission lines, but it is not

clear how much the gas contributes to the continuum emission. Rydgren, Strom, and Strom (1976) have suggested that the visual and infrared excesses are produced predominantly by free-free radiation by the hot gas, and that dust emission becomes significant

only at 10 and 20 μ m.

This model of T Tauri stars does not fit the observations of many of the stars unless a highly abnormal reddening law is postulated. As noted in § V, there seems to be no direct evidence for such an abnormal law. Additional evidence against this model is provided by infrared spectroscopy (Cohen 1975; Paper II; Fig. 3), as there are no definite detections of emission lines in any T Tauri stars. The upper limits on the equivalent width of B_{γ} in emission are typically ~ 5 Å. Although self-absorption will reduce the emission-line strengths below those expected from optically thin recombination, it seems plausible that much of the 2 μ m emission is in fact from hot dust.

The $2 \mu m$ spectra of these objects are not wholly featureless. Hubble 4 (object 22) and the binary star UZ Tau (object 11) both show weak CO and H₂O absorption features (Fig. 3). Hubble 4 has a negligible $2 \mu m$ excess, and the strengths of the absorptions can be compared with those predicted from the visual spectral type of K7, assigned by Herbig (1977). The strengths of the absorptions are consistent with that of a dwarf of spectral type M0 or M1 (Persson, Aaronson, and Frogel 1977), although a real surface gravity determination is not possible. In UZ Tau, the 2 μ m excess is significant, and the true absorption band strengths cannot be determined easily. The strengths observed are consistent with Herbig's (1977) visual spectral types of the system, between M1 V and M4 V, if the circumstellar emission is comparable in strength to the stellar emission. The presence of the CO and H₂O features supports the general picture of the T Tauri stars as cool stars with moderate surface gravities (Herbig 1977; Mould and Wallis 1977).

X. COMPARISON OF THE OPHIUCHUS AND TAURUS DARK CLOUDS

a) Observed Properties

A comparison of the properties of the two major dark cloud complexes in Ophiuchus and in Taurus is of considerable interest, as both dark cloud complexes are of roughly similar extent, and are at very similar distances (160 pc for Ophiuchus, 140 pc for Taurus [Appendix A]). The two regions are nonetheless quite different, both in their morphology and in their apparent stellar content. Such a comparison has been previously made by Rydgren, Strom, and Strom (1976) and by Vrba (1977), who also proposed explanations for the observed differences. The new data presented in this paper for Taurus, and in Paper II for Ophiuchus, permit strengthening or modification of the conclusions presented by Rydgren et al. and by Vrba.

The most noticeable difference between the two regions is the paucity of OB stars in Taurus compared to Ophiuchus, already noted by Strom, Strom, and

Grasdalen (1975). This difference applies primarily in the immediate vicinity of the dark clouds, where most of the recent star formation has presumably occurred. In Ophiuchus one sees close to twenty B or A0 stars in the immediate vicinity of the dark clouds (Paper II), whereas in Taurus there are only two early-type stars inside the region studied in this paper (objects 1 and 18). One more early-type star, AB Aur (Strom, Strom, and Vrba 1976), is found in dark cloud material farther to the east.

A similar difference is not seen if one compares the T Tauri star populations; in fact, there may be more such objects detected in the Taurus survey than in Ophiuchus (Paper II), although T Tauri star identifications in both regions are incomplete.

Comparisons between populations of more exotic objects indicate that there are peculiar objects unique to each cloud. In particular, the Ophiuchus region contains a number of very red objects surrounded by reflection nebulae; such objects appear absent from Taurus. In contrast, Herbig-Haro objects are found

in Taurus but not in Ophiuchus.

In addition to the differences in the stellar populations of the two regions, there are differences in the morphology of the clouds and of the star formation regions within them. The newly formed stars in Ophiuchus appear strongly concentrated in a region a few parsecs across (Rydgren, Strom, and Strom 1976; Paper II), while in Taurus the young objects are distributed over a far larger region (§ IV). The dark clouds themselves appear different: the Taurus clouds appear far more patchy and fragmented than the clouds in Ophiuchus. This is not because the Taurus clouds are less opaque, since they include regions with inferred visual extinctions of ~20 mag (near objects 15 and 18, for example) whereas the typical visual extinction in Ophiuchus is probably not much greater than 10 mag (Paper II).

b) Interpretation

The differences observed between the Taurus and Ophiuchus regions imply that recent star formation in Taurus has been more widespread, but has generally resulted in stars of lower mass. There are at least two possible explanations for this fact. The first is that the Taurus clouds are younger than the Ophiuchus region, and that in the future the stellar population in Taurus will resemble that in Ophiuchus, while an alternative is that the star formation mechanisms in the two regions are qualitatively different. Of these, the second explanation appears most consistent with the evidence.

Vrba (1977) has discussed the situation in Ophiuchus. He argues that the magnetic field geometry (Vrba, Strom, and Strom 1976) and the position of the most recently formed stars at the western edge of the dark cloud complex suggest that these stars have formed in a part of the cloud compressed by a shock propagating through the cloud. According to this picture, the prominent streamers which extend eastward from the cloud represent material ejected along

magnetic field lines by the shock. Carbon monoxide velocities of these streamers relative to the main cloud were used to estimate approximate ages of $5-7 \times 10^6$ years. This age is consistent with that of the youngest B stars (e.g., Stothers 1972). Many of the pre-mainsequence stars in the central regions of the cloud appear to be significantly younger than this (e.g., Rydgren, Strom, and Strom 1976; Paper II). This suggests that the event which triggered star formation in the central region of the cloud postdates the formation of the streamers and the observed main-sequence B stars. It is tempting to speculate that the event (such as a supernova [Herbst and Assousa 1977]) which triggered the most recent episode of star formation is the same as that which produced the runaway star ζ Oph; this event is estimated to have occurred $\sim 10^6$ years ago (Blauuw 1961; Stothers 1972).

In Taurus, the widespread star formation and the absence of high-mass stars suggest that the recent star formation has been spontaneous and has not been triggered by an external event (cf. Elmegreen and Lada 1977; Vrba 1977). This is also consistent with the extremely fragmentary appearance of the Taurus clouds and the absence of any preferred regions where star formation is occurring.

The Taurus and Ophiuchus regions thus appear completely different; their past histories have probably also been quite different. Although their futures are unclear, it seems reasonable that the differences in cloud morphology and in associated stellar population will cause their future evolution to continue to diverge.

XI. CONCLUSIONS

Two general results emerge from this study of the Taurus region. The first is that recent star formation

has occurred in many locations in the cloud; while there are small clusterings of young objects, there is no single site where almost all recent star formation has happened. The second result is that the stellar population is dominated by T Tauri stars and similar objects, although there are a few more luminous objects in the region studied.

A number of interesting objects have been identified in this work. These include a new Herbig Ae star in the IC 359 region (object 1) and a probable new Herbig-Haro object, Haro 6-10 (object 7). Studies of object 1 and of the star illuminating IC 2087 (object 18; Allen 1972) indicate that these have significant infrared excesses at wavelengths as short as $2.2 \,\mu\text{m}$. Observations of Haro 6-10 in the infrared show it to be intrinsically cool and quite variable. These results were derived using a reddening law determined from measurements of field stars obscured by dark cloud material; this law appears no different in the infrared from that seen in the Ophiuchus region or in the interstellar medium.

Comparison of the Taurus region to the Ophiuchus dark cloud complex strongly suggests that the two are qualitatively different, and that the dominant star formation mechanisms in each are different.

This work would not have been possible without the aid of the Mt. Wilson night assistants, J. Frazier, H. Lanning, and E. Hancock, and help from other members of the Caltech infrared group, especially D. Nadeau, S. Beckwith, and A. Sargent. G. Neugebauer provided a number of useful discussions. This work was partially supported by National Science Foundation grant AST 74-18555A2, National Aeronautics and Space Administration grant NGL 05-002-207, and by the California Institute of Technology.

APPENDIX

DISTANCE TO THE TAURUS DARK CLOUDS

Three different methods have been used to find the distance to the Taurus dark clouds. The first method uses observed star counts versus magnitude to find both a distance and a mean absorption due to intervening material. This method has been applied by Greenstein (1937) and McCuskey (1939), who find a distance of 140 pc. In the second method the reddening of field stars is plotted as a function of their distance; large changes in the reddening occur at the distance of the reddening material. Gottlieb and Upson (1969) have used this approach to find an approximate distance of 150 pc.

The third method is to find the distances to stars known to be associated with the dark cloud material; this method clearly works only if the stellar luminosities are well known. Van den Bergh (1966) has assembled a catalog of bright stars associated with nebulosity which includes several stars in Taurus; Racine (1968) has found the distances to these objects using spectroscopy and visual photometry. Racine ob-

tains a distance of 135 ± 10 pc for the Taurus dark clouds, based on stars spread over a large area. If the stars are restricted to a smaller area, and if the B7 star 72 Tau (Dorschner and Gürtler 1963) is added, a

TABLE 6
TAURUS DARK CLOUD DISTANCE

HD	Spectral Type	$(m-M)_0$
26154 28149 30378 31293 Mean	G6 III* B7 V† B9.5 V* A0ep*	5.3* 6.0† 5.9* 5.4* 5.65 ± 0.2

^{*} Spectral type and distance modulus from Racine 1968.

[†] Spectral type and distance modulus from Lesh 1968.

872 ELIAS

distance of 135 ± 15 pc results (Table 6). The different estimates of the distance to the Taurus dark cloud are all in good agreement. The mean of these estimates is roughly 140 pc; this value has been used in this paper. Although the different distance estimates

agree to better than 10%, it seems reasonable to believe that the radial extent of the dark cloud complex is comparable to its projected extent of $\sim 10^{\circ}$ or 25 pc. The distances of individual objects are therefore probably uncertain by roughly ± 20 pc.

REFERENCES

J. H. ELIAS: Cerro Tololo Inter-American Observatory, Casilla 63-D, La Serena, Chile

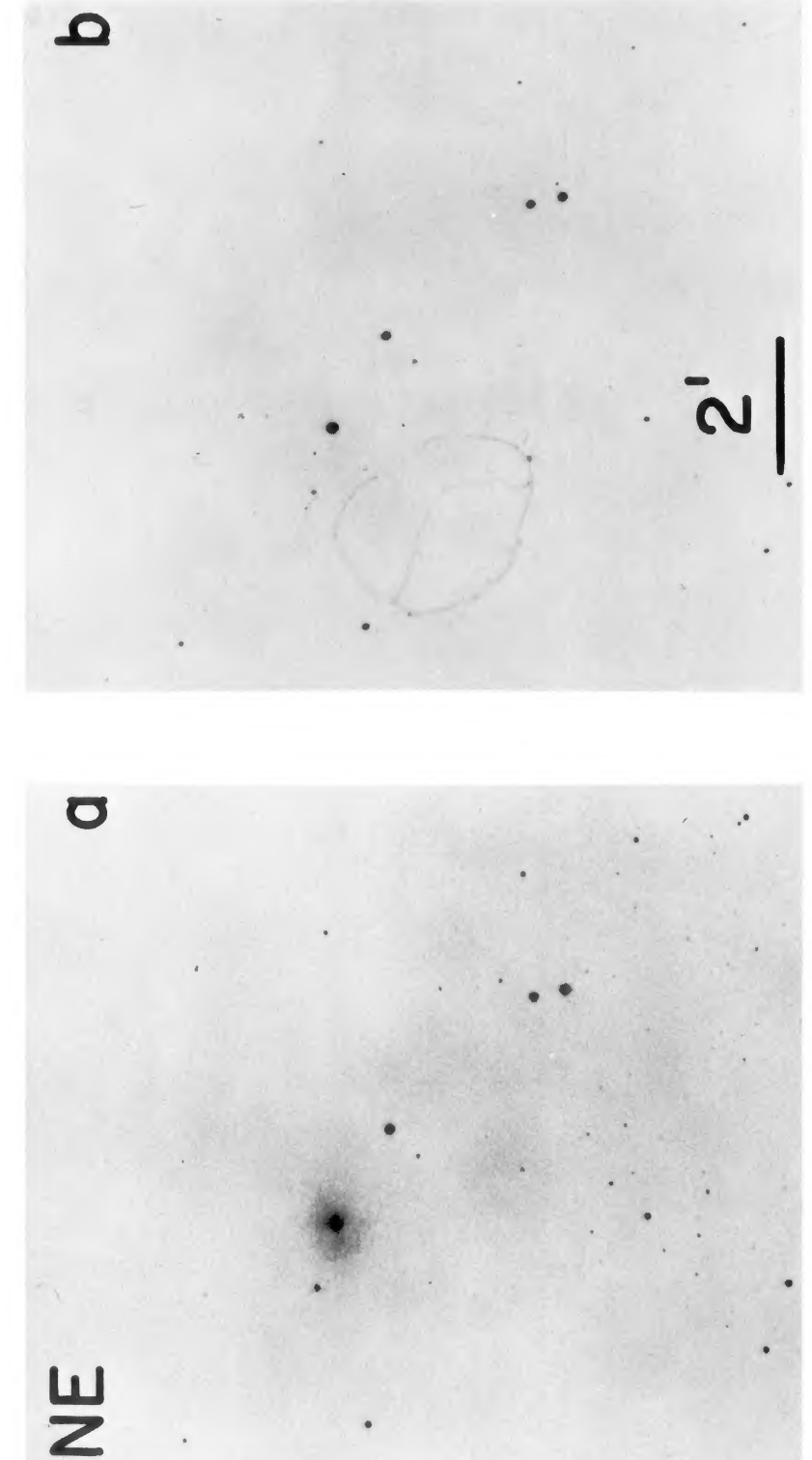
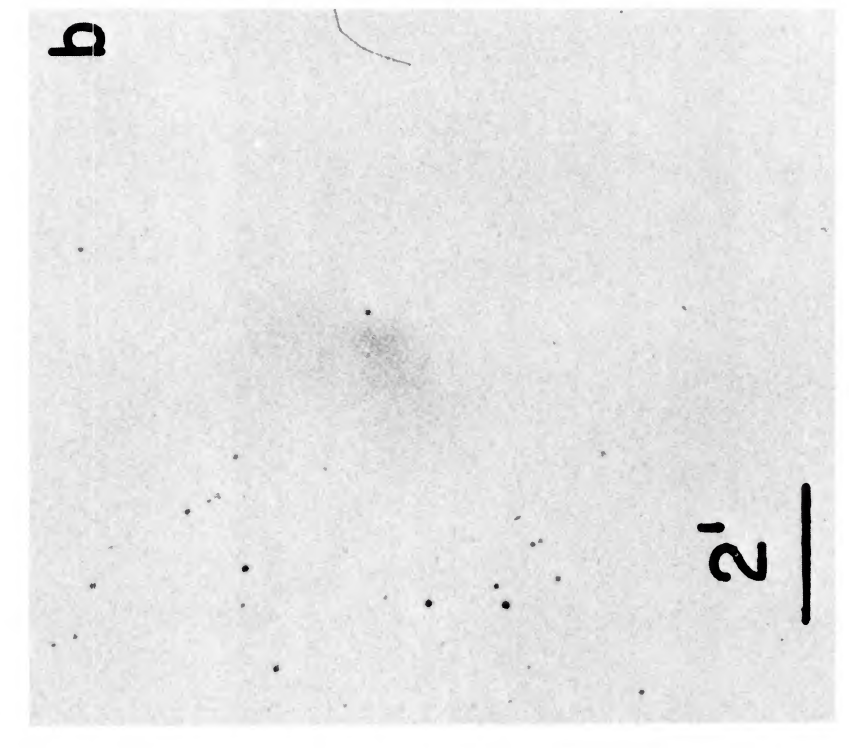


Fig. 5.—Photographs of the IC 359 region. North is to the top, east is to the left. The left-hand photograph is a red (127-04) plate, and the right-hand photograph is an infrared (IV-N) plate. Hubble 4 is the bright star in nebulosity northeast of the center, object 1 is the central object, and CZ and DD Tauri are the two stars to the southwest.



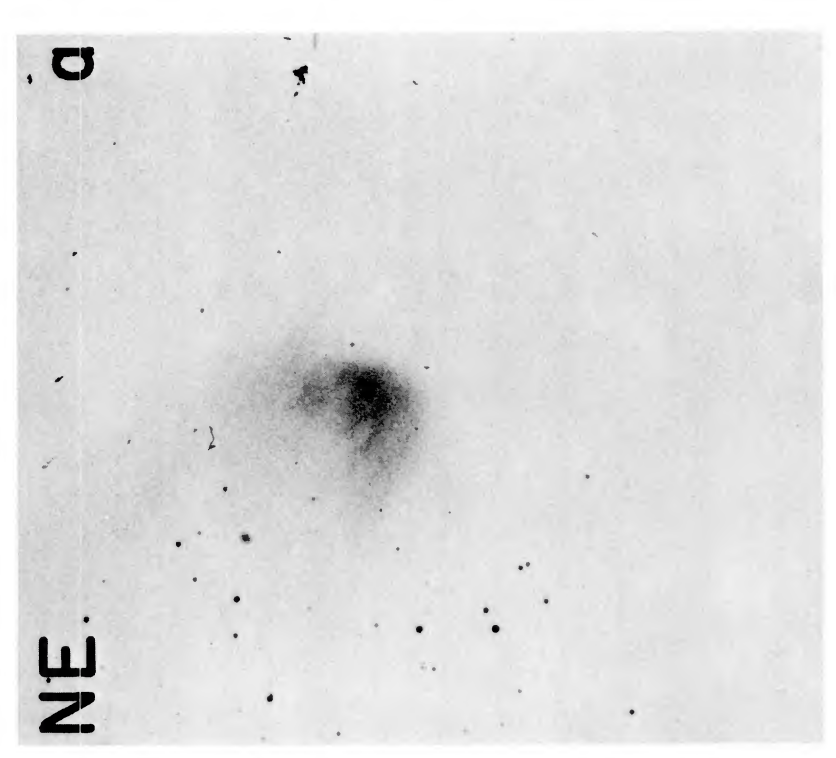


Fig. 9.—Photographs of the IC 2087 region. The left-hand photograph is a red (127-04) plate, and the right-hand photograph is an infrared (IV-N) plate. The star (object 18) presumed to be illuminating the nebula is seen about 20" west of the nebulosity.

ELIAS (see page 866)

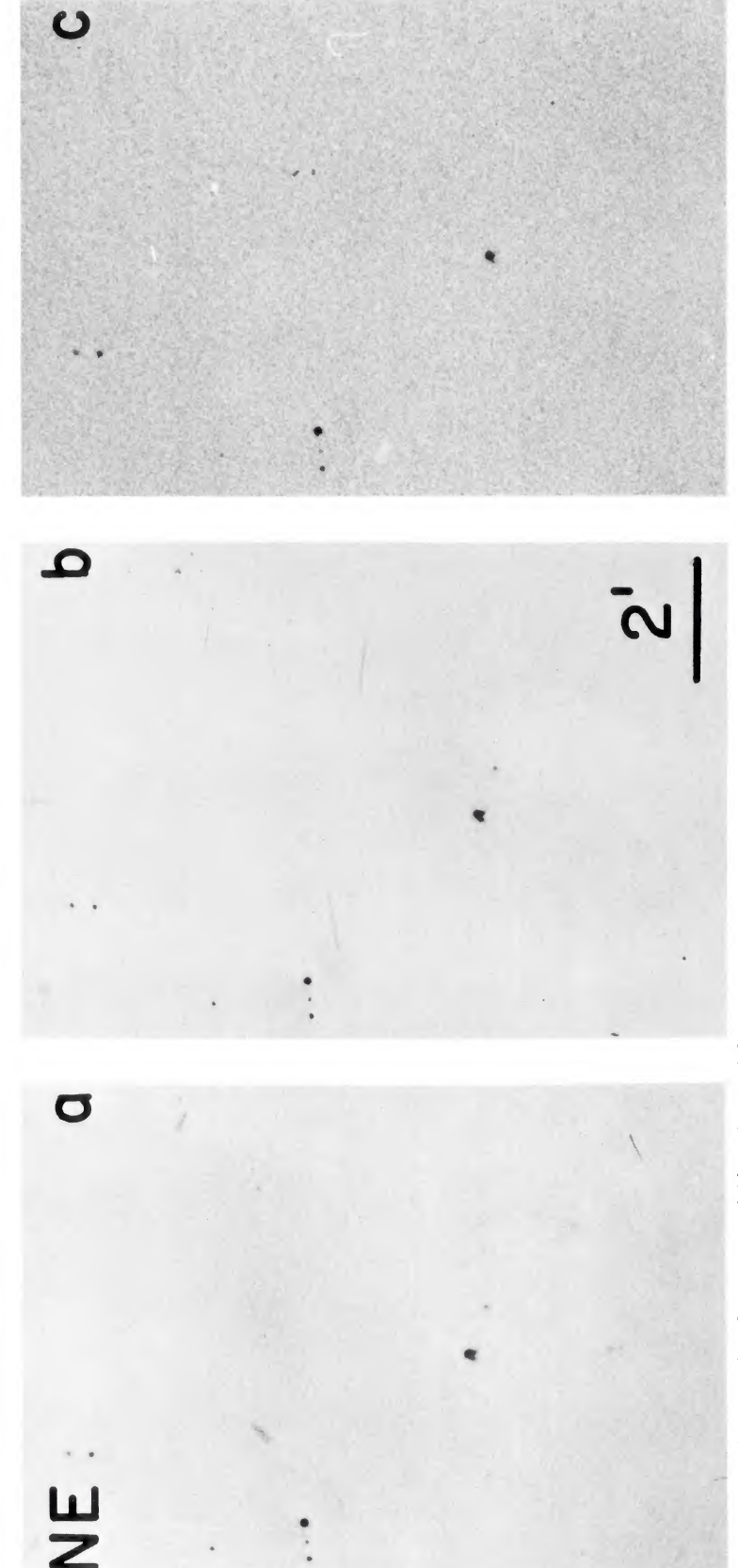


Fig. 12.—Photographs of Haro 6-10 (object 7). The left-hand two photographs are red (127-04) plates, taken in 1976 February and November, respectively, while the rightmost photograph is an infrared (IV-N) plate taken in 1976 October. Haro 6-10 is the nonstellar object slightly below center. Note the wisp 1' to the west. ELIAS (see page 867)